Nucl. Sci. and Tech., Vol.12, No. 4 (2022), pp. 29-37

Nuclear Science and Technology

Journal homepage: http://jnst.vn/index.php/nst

Research and manufacture of the mini gamma camera using multi-anode photo multiplier tube (Ma-PMT)

B. N. Ha[1], N. T. Hoang, D. N. T. Duy[2], L. V. Hai[2], V. T. Trang[3]

[1] *Hanoi University of Science and Technology*
[2] *Center for Applications of Nuclear Technique in Industry*
[3] *ThuongMai University*
Email: ha.buingoc@hust.edu.vn, theduy@canti.vn

Abstract: A Gamma camera is an imaging technique that captures gamma radiation emitting from radiation sources. In this paper, the authors built a Mini-Gamma camera system using a micro photo-multiplier tube (µPMT) H12700, signal processing circuit, and control software as self-designed products. The Gamma camera system includes four parts: i) collimator, ii) scintillator NaI(Tl), iii) µPMT, and iv) processing and controller boards. The electronic system uses a pre-amplifier to amplify and convert negative signals from the µPMT to positive ones. An integrator circuit is used to sharpen the signal from the pre-amplifier, and an amplifier circuit is used to amplify the signal from the pre-amplifier. Finally, the position detection circuit is utilized to detect the location of radiation interaction in the detector head. All circuits in the Mini-Gamma camera system are optimized to increase the spatial resolution of the projection. In this work, the lab-built Mini-Gamma Camera has an energy resolution of 45% at 60 keV gamma rays, the affected field of the camera is 42×48.5 mm^2, and the spatial resolution of the image is around 1 mm.

Keywords: *Ma-PMT, Gamma camera, Compton Camera, nuclear imaging technique, H12700.*

I. INTRODUCTION

The transmission imaging method known as the gamma camera, or Anger camera, has several uses. In order to identify radioactive hotspots, gamma cameras may be utilized in nuclear site decommissioning, homeland security, and medical imaging. In the 1950s, American Hal O. Anger created the Gamma Camera system for nuclear medicine imaging at Donner Laboratory in Berkeley, California. To absorb and transform gamma rays into visible light for the Anger camera, a monolithic scintillator is used. In order to ascertain the interaction location of incoming radiations and their absorbed energy in the scintillator, visible light generated by the scintillator is then detected by the Photo Multiplier Tube (PMT) matrix. By keeping track of the location data, one may create an interaction history map of incoming radiation, which is analogous to an intensity distribution of the radiation source or a projection picture of the item beneath the radiation field [1]. Gamma cameras are now typical components of nuclear medicine diagnostic systems like single-photon emission computed tomography (SPECT) and positron emission tomography (PET) [2–6].

Recently, several research groups in the world developed a small Gamma Camera for research and clinical applications [7-10]. Unlike a normal Gamma Camera, Mini-Gamma Camera can acquire useful images in a short time and can move around the patient to observe interesting nodes or areas. In 2003 F. Sanchez et

https://doi.org/10.53747/nst.v12i4.375
Received 25 November 2022, accepted 11 October 2022

al. successfully built a portable gamma camera using a position-sensitive photo-multiplier tube (PSMPT). This PSMPT has dimensions of 90 mm × 200 mm (diameter × length), 2 mm spatial resolution, and 13% energy resolution at 140 keV [7]. In the meantime, M. M. Fernandez et al. developed a mini gamma camera using the H8500 Multi-Anode Photomultiplier Tube (Ma-PMT) of Hamamatsu Photonics. In comparison with F. Sanchez's work, the mini gamma camera of M. M. Fernandez has a larger effect field of 70×70 mm^2 and better spatial resolution (1.5 mm) [8]. In 2014, Olcott et al. used a mini gamma camera to evaluate sentinel lymph node biopsy. Olcott used a gamma camera with a spatial resolution of about 1.8 mm and an energy resolution of 12% at 140 keV [9]. Also, in 2014, Knoll et al. successfully manufactured a portable gamma camera using a 40 mm × 40 mm × 5 mm cadmium-zinc-telluride (CZT) detector. That gamma camera can take a transmission image of the object with a spatial resolution of 2 mm, and an average energy resolution of 5.2% at 140 keV [10].

All gamma cameras from previous research are used in clinical; they employ high-performance ADC cards combined with a personal computer to digitalize analog signals and display images. Therefore, that systems consume high power and increase the manufacturing cost. In this research, we design the mini-gamma camera system using analog-digital converter ADC on Microcontroller (MCU) and high sensitivity Hamamatsu Photonics H12700 Ma-PMT couple with a NaI(Tl) scintillator. Our system has lower power consumption so that it can work for a long time with the battery. It can be used in industrial or medical SPECT techniques in facilities without the main power. The signal processing circuits and controller programs in this research are designed and optimized in our laboratory to fit ADC on MCU and increase the spatial resolution of the image.

II. SUBJECTS AND METHODS

Figure 1 shows the mini-gamma camera system's block diagram built in this research; it consists of detector head block, position detection and pre-amplifier block, signal processing block, and MCU and displayer block. The detector head is constructed by the Hamamatsu H12700 Ma-MPT and a NaI(Tl) scintillator with dimensions of 50 mm x 50 mm x 8 mm. Each micro photo-multiplier tube in the H12700 Ma-PMT is around 6 mm by 6 mm and is arranged in an array to provide an active area of 48.5 mm by 48.5 mm [13].

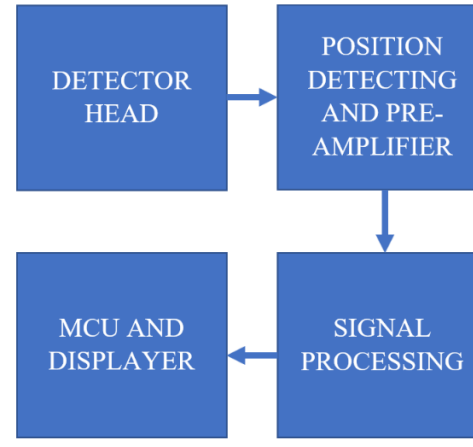

Fig. 1. Block diagram of mini-gamma camera system

The radiation detection block gathers and processes the H12700 Ma-PMT's electrical signals. The spatial resolution of the image will be pretty low if signals from each micro PMT are only considered to be signals from a single pixel. To improve spatial resolution, 64 Ma-PMT outputs are linked to a resistor network known as a position-detecting circuit. Several nearby micro PMTs gather the

visible light created by the interaction of incoming radiations with the scintillator, producing electronic signals with amplitudes that depend on the location of the radiation interactions. Four output signals, A, B, C, and D (Figure 2), are created at the network's output from the electronic signals input into the resistor network. Formula 1 is used to determine the coordinate of interaction position of radiation on the scintillator (the origin point of the visible light beam) using the A, B, C, and D signals, which are referred to as position-sensitive signals [13].

$$x = \frac{A+C}{A+B+C+D}$$
$$y = \frac{C+D}{A+B+C+D} \quad (1)$$

The architecture of the resistor network employed in this study is shown in Figure 2. Depending on the consistency of the internal electron magnification of the micro PMTs, the resistor value in the network should be adjusted. One may make the output signal more homogenous and less distorted by modifying the resistor to account for the variance in internal electron magnification in each micro PMT.

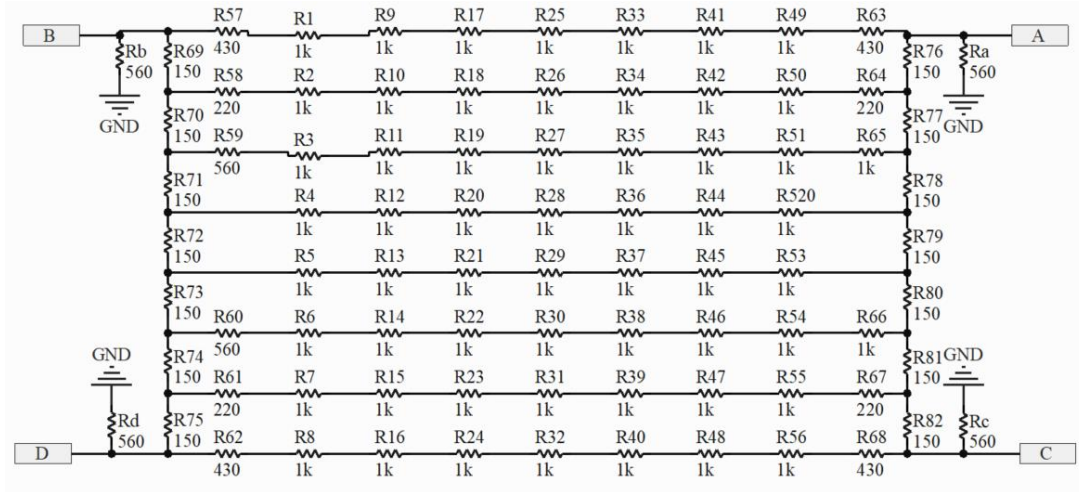

Fig. 2. Schematic of the position detection circuit

The small-amplitude, negative signals A, B, C, and D are position-sensitive signals. To convert negative signals into positive signals and reduce noise and signal application, a four-channel pre-amplifier is used. A four-channel acquisition and processing circuit provide amplified position-sensitive signals. Figure 3 displays the design for each acquisition and processing channel. Each channel includes an integration circuit (low pass filter circuit), amplifier circuit, and peak detection circuit. The shaping circuit, also known as the integration circuit, is used to shape signals and improve their signal-to-noise ratio. Formula 2 displays the phase shift of the circuit as well as the integrator's cut-off frequency.

$$f_c = \frac{1}{2\pi.R.C} = \frac{1}{2\pi.300.47.10^{-9}} = 11287.6(Hz)$$
$$\varphi = -\arctan(2\pi.R.C.f_c) = \frac{\pi}{4}(Rad) \quad (2)$$

Positive pulses are created by feeding signals from the four channels A, B, C, and D into the non-inverting amplifier circuit with a gain of 50. To determine the interaction location of the gamma-ray on the Ma-PMT, these positive signals are supplied into the ADC via the buffer. The interactive radiation map, equal to the distribution of radiation sources or

projection images of the sample in radiation photography methods, may be made after collecting the location of the interaction of incoming radiation.

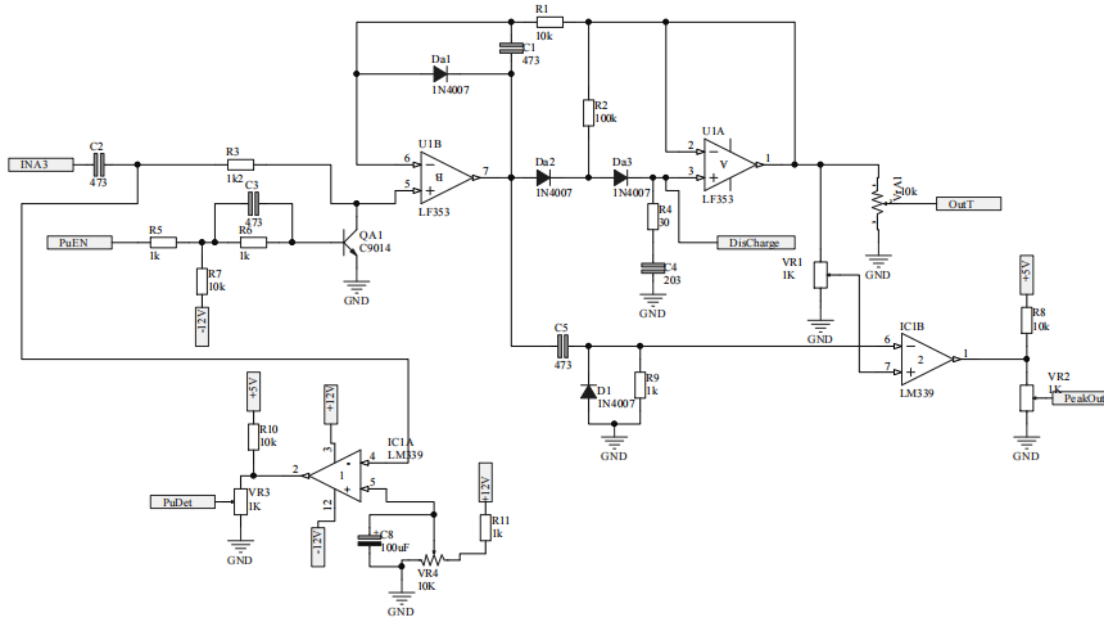

Fig. 3. Schematic of one channel in the signal processing circuit

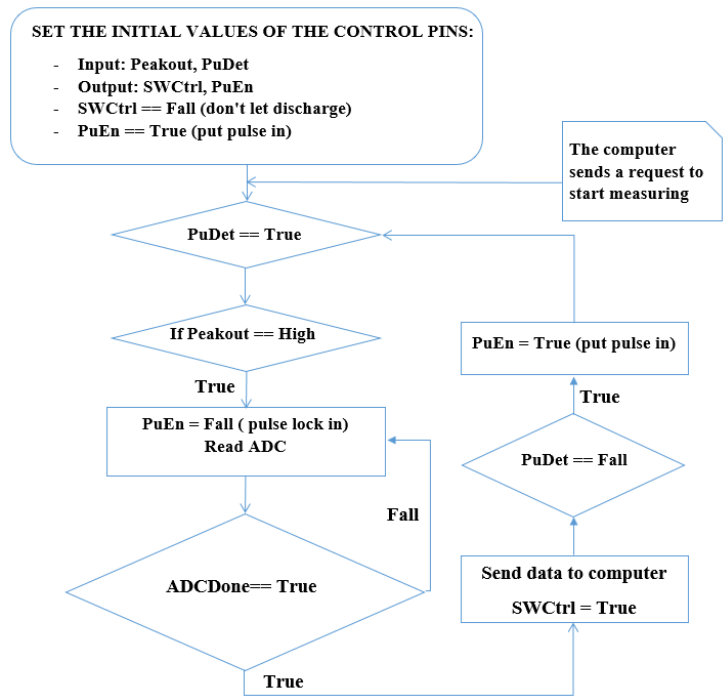

Fig. 4. Algorithm diagram of controller program

Figure 4 shows how the signal processing circuit's schematic design served as the foundation for the microcontroller algorithm. The computer sends the request to start the measurement after initializing the control settings and launching the program. To

ascertain whether the radiation interaction has taken place or not, the control software, which is executed on a microcontroller, waits for the incoming notification signal "PuDet." The microcontroller waits for the peak detection signal "Peakout" if the radiation interaction occurs. Next, four channels ADC read the peak amplitude of the incoming pulse which is stored on the memory capacitor of the processing circuit. The microcontroller resets "PuEn" signal while the ADC reads and converts the amplitude signal to stop undesired events from entering the processing circuit. The controller transmits the digital signal to the computer and sets "PuEn" to be ready for the next measurement when the ADC conversion is complete. Until the controller gets the computer's finishing signal, the measuring procedure will be repeated.

III. RESULTS AND DISCUSSION

A. Results

The output signals from the radiation detection block and the pre-amplifier is shown in figure 5.

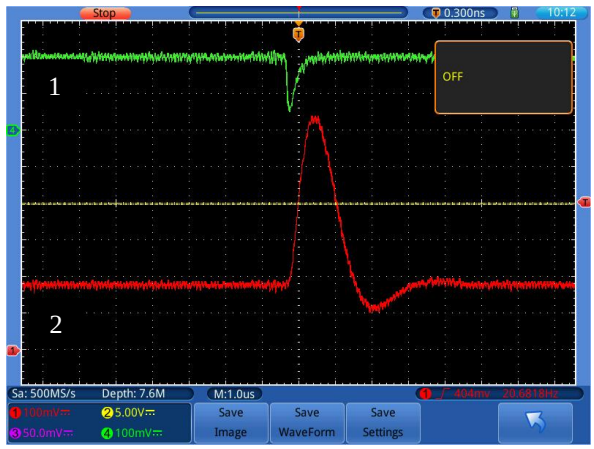

Fig. 5. The signal from position detection circuit (1) and pre-amplifier circuit (2)

Figure 6 shows the waveform of the output signal at the input gate of the signal processing circuit (1), the output of the amplifier (2), the output of the peak detector circuit (3), and the input of ADC (4).

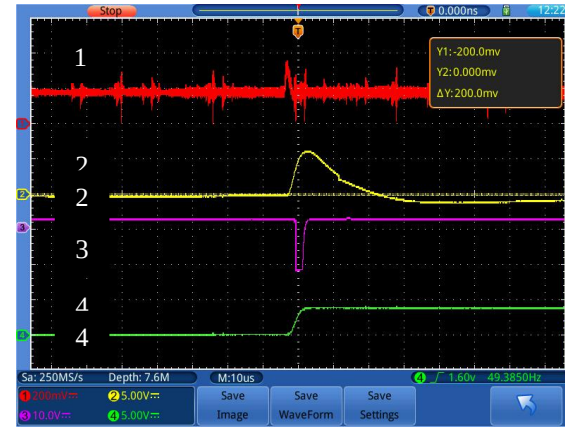

Fig. 6. The input signal (1); the amplified signal (2); the peak detection signal (3), and the ADC input signal (4)

Figure 7 displays the radiation spectrum of Am-241 source measured by a lab-built mini-gamma camera.

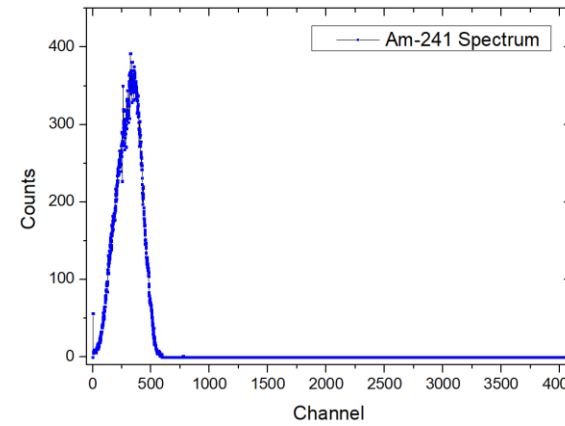

Fig. 7. Pulse height spectrum of the Americium 241 (uniform) source

Figure 8 describes the center of the interactive position of the radiation source, measured with a collimator that has 0.6 mm in diameter. The gain of four amplifiers is set to the same value.

Figure 9 depicts the distribution of radiation source when translated on the surface of the detector with the movement step of 0.6 mm.

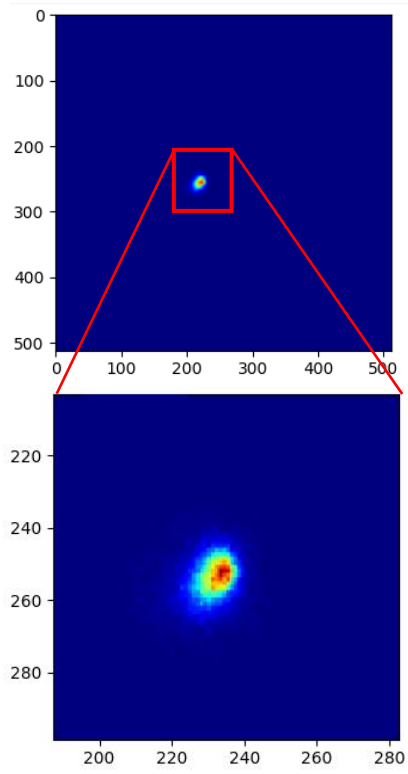

Fig. 8. Calibration results of 4-channel A, B, C, and D signal when placing radioactive source at the center of the detector plane

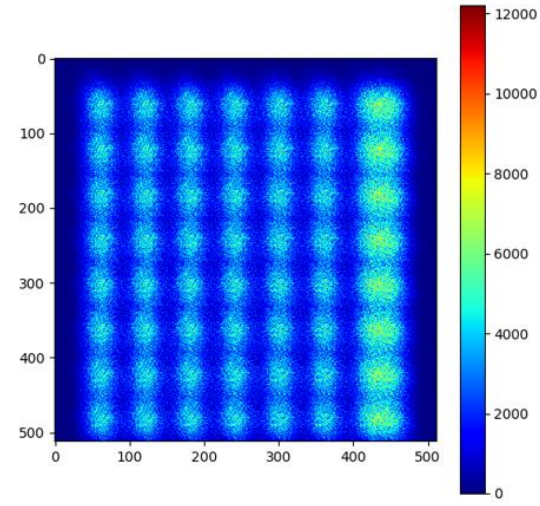

Fig. 9. Position reconstruction

Figures 10 and 11 show the projection images of two simple samples, which are captured using a mini-gamma camera with an integration time of 2 minutes.

Table I describes the measured dimension of the object in the projection image in comparison with the real one of the two samples in Figures 10 and 11.

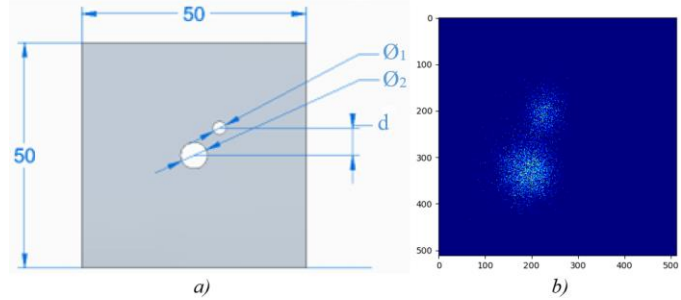

Fig. 10. a) capture sample 1, b) capture image of sample 1

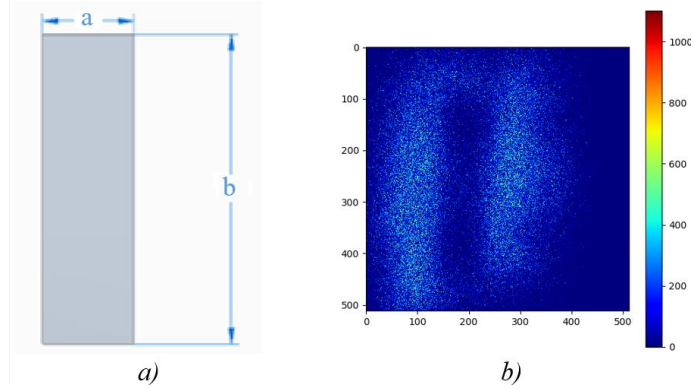

Fig. 11. a) sample 2, b) image is taken from sample 2

Table I. The samples and images information; Components of the samples are presented

Sample	Manufacturing size (mm)	Measured size (mm)
Sample 1	$Ø_1$: 6.04 ± 0.32 mm	$Ø_1$: 5.88 ± 0.70 mm
	$Ø_2$: 3.02 ± 0.14 mm	Ø2: 2.94 ± 0.56 mm
	d: 6.36 ± 0.10 mm	d: 6.02 ± 0.66 mm
Sample 2	a: 27.10 ± 0.12 mm b: 8.16 ± 0.22 mm	a: 28.00 ± 0.74 mm b: 9.07 ± 0.76 mm

B. Discussion

Figures 5 and 6 show that the pre-amplifier's amplitude gain is exactly three times what it was in the original design. If we closely examine the two figures, we can see that the output pulse width of the pre-amplifier is around 1.6 s, and the output signal has a greater signal-to-noise ratio than the input signal. The pulse width of the amplifier's output signal is about 30 s, and it has the same phase as the pre-amplifier's output signal. As a result, the processing circuit can process data at a maximum rate of 33 kHz, which is a respectable processing speed for a lab-built pulse processing electronic system. The system's overall speed is slowed down to less than 10 kHz by the low-speed ADC, which has a conversion time of up to 100 s (shown in Figures 4 and 6).

The Gamma camera works well when detecting incoming gamma rays with energy ranging from 50 keV to 200 keV; most other studies performed gamma camera image records using 140 keV gamma rays. To assess the performance of the mini-camera system, we must employ Am-241 since it is not feasible to use the Tc-99m isotope source (140 keV gamma emission) in this research. The radiation spectrum of the Am-241 source is shown in Figure 7. As can be seen, across 4000 channels of the spectrum, the photoelectric peak begins between Channels 0 and 600. Due to electrical noise, several of the early channels in the spectrum have large counts. The numbers that result from noise are not as high, however. We may take out the first five spectral channels to improve the accuracy of the estimation of the radiation position's interaction. The energy resolution of Am-241 peaks is around 45%; further research is required, particularly utilizing the Tc-99m source, to compare the mini-gamma camera's energy resolution to the findings of the other group.

Because the gain distribution of Ma-PMTs is not uniform. Therefore, we must correct the position detection circuit (resistor network) in conjunction with a gain coefficient of four channels to ensure that the output signal must be equal when the radiation source is positioned at the center of the scintillator's surface in order to precisely calculate the position's interaction of incoming radiation. Figure 8's outcome demonstrates that when the source is positioned in the scintillator's center, the recorded source's position's coordinates are X = 230 and Y = 250, with 500 being the highest value of X and Y. As a result, we can see that the interaction's position is constrained along the X-axis. The calculated value of X from formula (1) must be multiplied by factor 25/23 in order to achieve a 1:1 ratio between the X and Y axes. The translational picture of the radiation source in figure 9 demonstrates that, after correcting the calculated location, we were able to produce an image that fairly accurately depicted the source's position. In the 7×8 area of the matrix of source points, the source distances are evenly distributed along

the X and Y axes. The position of the sources is almost overlapped in the seventh and eighth columns. As a result, when the source travels to the seventh column position, the estimated value of X does not move linearly with the actual value of X. The cause of this problem may be due to the unevenly distributed internal gain of the Ma-PMT, or the border area of the scintillator has a distortion that prevents it to function properly. As a result, the actual radiation-recorded active area, which corresponds to 42.0 mm × 48.5 mm, is only 7×8 points.

Figures 10 and 11 show the imaging outcome of two simple objects captured by the Gamma Camera system after correcting the position detection formula. The result demonstrates that the shape of two objects is clearly displayed in the image; we can calculate the size of the actual object by using that projection image. Table I presents the comparison between the calculated and actual sample sizes. Sample 1 is shaped like a hole; hence the size measured on the picture will be less than the real thing since the object scatters radiation. Sample 2 is a solid rectangular item, in contrast, and since radiation tends to scatter outward, the size of the object seems greater in the picture than it really is. The sample's actual size and the size that was measured deviate by less than 1 mm. Consequently, the mini-Gamma Camera system has a spatial resolution of around 1 mm.

IV. CONCLUSION

In this work, a multi-Anode Photo-multiplier tube H12700 combined with a NaI(Tl) scintillation crystal was successfully used to create a mini-Gamma Camera system. The system's other components, including the pre-amplifier, signal collection and processing, and control software, are created in-house at our lab. With a 10 kHz data processing speed, a 42 mm x 48.5 mm effective field, a 45 percent energy resolution for 60 keV gamma-ray energies, and a 1 mm spatial resolution, this mini-Gamma Camera system offers all the specifications which are suitable for the mini-SPECT system for pre-clinical use that is being researched and manufactured in Center for Applications of Nuclear technique in Industry.

By using a quicker ADC and high-speed signal processing to speed up the data collection process, we boost the gamma camera system's recording speed in future research. We will test the device using a Tc-99m radiation source to learn more about the detector's energy resolution. In order to improve the effective field of recording of the device system, we plan to create 64 pre-amplifiers and mount them directly on each photo-multiplier tube to take into account the change in the internal gain of the photo-multiplier tubes.

ACKNOWLEDGMENTS

The work was carried out under the framework of the Ministry of Science and Technology project No. ĐTCB.04/20/TTUDKTHN.

REFERENCES

[1]. Jerrold T. Bushberg, J. Anthony Seibert, Edwin M. Leidholdt Jr., John M. Boon, *The Essential Physics of Medical Imaging*, 675-680, 2002.

[2]. Cardona-Arboniés J, Mucientes-Rasilla J, Moreno Elola-Olaso A, Salazar-Andía G, Prieto-Soriano A, Chicharo de Freitas J, *Contribution of the portable gamma camera to detect the sentinel node in breast cancer during surgery*, Revista Española de Medicina Nuclear e Imagen Molecular;31:130–4, 2012.

[3]. Ferretti A, Chondrogiannis S, Marcolongo A, Rubello D., *Phantom study of a new*

hand-held c-imaging probe for radio-guided surgery, Nuclear Medicine Communications; 34:86–90, 2013.

[4]. Bugby SL, Lees JE, Bhatia BS, Perkins AC., *Characterization of a small high-resolution field of view portable gamma camera*, Physica Medica; 30:331–9, 2014.

[5]. Tsuchimochi M, Hayama K., *Intraoperative gamma cameras for radio-guided surgery: technical characteristics, performance parameters, and clinical applications*, Physica Medica; 29:126–38, 2013.

[6]. Heller S, Zanzonico P., *Nuclear probes and intraoperative gamma cameras*, Seminars in Nuclear Medicine; 41:166–81, 2011.

[7]. Sanchez F, Benlloch J, Escat B, Pavón N, Porras E, Kadi-Hanifi D, *Design and tests of a portable mini gamma camera*, Medical Physics; 31:1384–97, 2004.

[8]. Fernández M, Benlloch J, Cerdá J, Escat B, Giménez E, Giménez M, *A flat-panel-based mini gamma camera for lymph nodes studies*, Nuclear Instruments and Methods in Physics, Research Section A; 527:92–6, 2004.

[9]. Trotta C, Massari R, Palermo N, Scopinaro F, Soluri A., *New high spatial resolution portable camera in medical imaging*, Nuclear Instruments and Methods in Physics, Research Section A; vol 577; pp604–10, 2007.

[10]. Knoll P, Mirzaei S, Schwenkenbecher K, Barthel T., *Performance evaluation of a solid-state detector based handheld gamma camera system*, Frontiers in Biomedical Technologies;1:61–7, 2014.

[11]. Lawson R.S., Jones D., Hogg P., Seeram E. (eds), *Practical SPECT/CT in Nuclear Medicine*, Springer, London, 2013, p47 https://doi.org/10.1007/978-1-4471-4703-9_.

[12]. Hammamatsu, *h12700_h14220_tpmh1379e*, 2019.